

## sPHENIX Conference Note

...

Measurement of the inclusive jet cross-section in  $p + p$  collisions  
at  $\sqrt{s} = 200$  GeV with the sPHENIX detector

The sPHENIX Collaboration

### Abstract

This sPHENIX Conference Note details the measurement of the inclusive jet cross-section as a function of transverse momentum ( $p_T$ ) in  $16.6 \text{ pb}^{-1}$  of proton-proton collisions at  $\sqrt{s} = 200$  GeV taken with the sPHENIX detector in 2024 at the Relativistic Heavy Ion Collider. Jets are reconstructed using the anti- $k_t$  algorithm with radius parameter  $R = 0.4$  using towers in the sPHENIX the electromagnetic, inner, and outer hadronic calorimeters. Kinematic selections on the jets include pseudorapidity  $|\eta| < 0.7$  and jet  $p_T > 15$  GeV. The Final cross-section is fully corrected for inefficiencies and unfolded for detector effects.

## 1 Introduction

Ultra-relativistic collisions of protons, like those that take place at the Relativistic Heavy-Ion Collider (RHIC) at Brookhaven National Laboratory (BNL) and the Large Hadron Collider (LHC) at CERN, can produce rare events in which hard scatterings between partons in the initial state give rise to highly energetic sprays of hadrons, known as jets. Jets are a phenomenon of quantum chromodynamics (QCD), and they act as faithful proxies for the partons that originated them at leading order [1]. Thus, the study of jet production allows one to access properties of quarks and gluons, objects typically constrained to the interior of hadrons via the confinement mechanism of QCD. Additionally, the suppression of the inclusive jet production cross-section is a fundamental measurement of jet quenching in the Quark-Gluon Plasma (QGP), for which measurements in proton-proton ( $p + p$ ) collisions serve as the baseline reference. The jet cross-section in 200 GeV  $p + p$  collisions at RHIC has been measured by the STAR [2] and PHENIX [3] experiments using the mid-point cone algorithm [4] and anti- $k_t$  [5] jets with radius parameter  $R = 0.3$ , respectively, and, additionally, a numerous of jet cross-section results have come from the LHC over the past decade [6, 7, 8].

This analysis note details the first measurement of the inclusive jet cross-section in  $\sqrt{s} = 200$  GeV  $p + p$  collisions at RHIC using jets measured by the sPHENIX full calorimeter system. Jets in sPHENIX are reconstructed using the anti- $k_t$  algorithm with a radius parameter of  $R = 0.4$  with inputs from both a high granularity electromagnetic calorimeter (EMCal) and, for the first time at RHIC at mid-rapidity, a hadronic calorimeter (HCal) to measure the neutral, hadronic components of the jet. The measurement is fully corrected for detector effects to the particle level using an unfolding procedure.

The data used in this analysis correspond to  $\mathcal{L} = 16.6 \text{ pb}^{-1}$  of the  $\sqrt{s} = 200$  GeV  $p + p$  dataset recorded in the 2024 RHIC operational period. This luminosity utilized here represents roughly 15% of that sampled over the entire Run 24  $p + p$  dataset. The inclusive jet cross-section as a function of the reconstructed jet  $p_T$ ,  $d\sigma/dp_T$ , is reported in the region  $|\eta| < 0.7$ .

## 2 sPHENIX detector

sPHENIX [9, 10] is a new detector designed to measure jet and heavy-flavor probes of the QGP created in Au+Au collisions at the Relativistic Heavy-Ion Collider (RHIC) [11]. A precision tracking system enables measurements of heavy-flavor and jet-substructure observables while the electromagnetic and hadronic calorimeter system is crucial for measuring the energy of jets and identifying direct photons and electrons.

Going outwards starting from the beam line, sPHENIX comprises the following subsystems [12]: the MAPS-based Vertex Detector (MVTX); the INTermediate Tracker (INTT); the Time Projection Chamber (TPC) [13]; the Time Projection Chamber Outer Tracker (TPOT) [14]; the Electromagnetic Calorimeter (EMCal) [15, 16]; the Inner Hadronic Calorimeter (IHCal) [16]; the 1.4 T superconducting solenoid magnet [17], and the Outer Hadronic Calorimeter (OHCal) [16]. Except for TPOT, all detectors have full azimuthal coverage and span  $|\eta| < 1.1$  in pseudorapidity. sPHENIX also includes a number of forward detectors, namely the Minimum Bias Detectors (MBD), the sPHENIX Event Plane Detectors (sEPD), and the Zero Degree Calorimeters (ZDC) which include

the Shower Maximum Detector (SMD).

sPHENIX began its commissioning process in RHIC Run-2023 with Au+Au collisions at  $\sqrt{s_{NN}} = 200$  GeV. During RHIC Run-2024, sPHENIX collected a large sample of transversely polarized  $p + p$  at  $\sqrt{s} = 200$  GeV physics data alongside a smaller sample of Au+Au data to complete its commissioning phase in that collision system.

### 3 Data and Simulation Samples

The data used in this analysis come from the RHIC 2024  $\sqrt{s_{NN}} = 200$  GeV  $p + p$  operational period. At the event level, there must be a successfully reconstructed z-vertex, provided by the MBD, and this reconstructed vertex must lie in the range  $|z| < 30$  cm, where  $z = 0$  corresponds to the center of the sPHENIX detector. Additionally, events must have fired a Level-1 jet trigger requiring that the event meets the standards of a minimum-bias (MB) event (meaning at least one PMT in the north and south arm of the MBD has received a hit above threshold) and additionally has a combined EMCal and HCal energy deposition above approximately 8 GeV in a region of  $\Delta\eta \times \Delta\phi = 0.8 \times 0.8$ . The event sample is further cleaned by selecting runs for optimal detector acceptance and minimum bias trigger performance. After these selections, which are chosen to harshly reject background events, the dataset analyzed here corresponds to  $16.6 \text{ pb}^{-1}$ , which is approximately one seventh of the total available luminosity in the Run-24  $p+p$  data-taking.

For corrections such as the jet energy scale calibration, unfolding, and jet and trigger efficiency corrections, PYTHIA-8 [18] simulations of  $\sqrt{s} = 200$  GeV  $p + p$  collisions with the Detroit tune [19] are generated, propagated through a full GEANT-4 [20] simulation of the sPHENIX detector and response, and reconstructed the same way as the data.

Three simulation samples are utilized:

- A Minimum Bias sample
- A Jet 10 GeV event sample with  $\hat{p}_T^{\text{min}} = 7$  GeV and a leading truth jet  $p_T$  cut of 10 GeV
- A Jet 30 GeV event sample with  $\hat{p}_T^{\text{min}} = 17.5$  GeV and a leading truth jet  $p_T$  cut of 30 GeV

Where  $\hat{p}_T^{\text{min}}$  is the minimum transverse momentum in the rest frame of the  $2 \rightarrow 2$  process for each of the products. The latter two datasets are generated with the options **HardQCD:all = on** and **PromptPhoton:all = on**. Additionally events in simulation have a z-vertex distribution that is Gaussian, centered at  $z = 0$ cm, and has a Gaussian width of 50 cm to match the z-vertex distribution in data. Jets at both the particle and detector level in simulation are clustered using the anti- $k_t$  algorithm and a jet radius of  $R = 0.4$ .

## 4 Analysis

### 4.1 Jet Reconstruction

Jets in sPHENIX are constructed from individual,  $\Delta\phi \times \Delta\eta = 0.1 \times 0.1$  towers from the inner and outer hadronic calorimeters, as well as re-towered EMCal towers of the same size. The re-towered EMCal towers are groups of EMCal towers that have been clustered together into a single object such that they match the segmentation of the hadronic calorimeters. These re-towered EMCal and the HCal towers serve as inputs for the anti- $k_t$  algorithm with radius parameter  $R = 0.4$ . No underlying event subtraction is performed at the time of reconstruction; rather, it is accounted for by the unfolding. Reconstructed jets are required to have a pseudorapidity such that the entire jet diameter is contained within the sPHENIX calorimetric acceptance in each calorimeter layer. For the event selection in this analysis requiring a z-vertex of  $|z| < 30$  cm, this is approximately equivalent to requiring that the reconstructed jet pseudorapidity,  $\eta^{\text{jet}}$ , be within  $\pm 0.7$ .

### 4.2 Background Rejection

In order to reject “fake” jets arising from beam-induced background events such as muons traversing the HCal scintillator and leaving large amounts of scintillation light, two methods are considered. The first method, the “energy fraction requirement method”, requires selections on the fraction of reconstructed jet energy found in the EMCal and HCal: the EMCal fraction,  $E_{\text{EMCal}}/E_{\text{Jet}}$ , must be between 10% and 90%, while the OHCAL fraction,  $E_{\text{OHCAL}}/E_{\text{Jet}}$ , must lie between 0% and 90%. This method introduces a correction for the selection inefficiency and is thus sensitive to the GEANT-4 modeling of the longitudinal shower deposition in simulation. The second method, the “dijet method”, includes a requirement on the presence of an additional jet in the event, approximately balanced in azimuth: the ratio of the subleading jet energy to the leading jet energy must exceed 0.3, and their azimuthal separation ( $\Delta\phi$ ) must be greater than  $3\pi/4$ . This method similarly introduces a correction for the selection inefficiency but is, instead, sensitive to the modeling of dijet topologies in the PYTHIA-8 simulation. The nominal results presented below are taken to be the average of these two methods, which are consistent with each other within 15%. The difference between the nominal the two methods is taken as a systematic uncertainty and is presented in Figure 4 in Section 5.

### 4.3 Trigger Efficiency Correction

To evaluate the trigger efficiency for each jet trigger threshold, the prescale-corrected jet spectra for the MB trigger and the jet trigger in question were divided, and the ratios are then fit by a sigmoid function to extract the efficiency as a function of jet  $p_T$ , as shown in Figure 1 on the left.

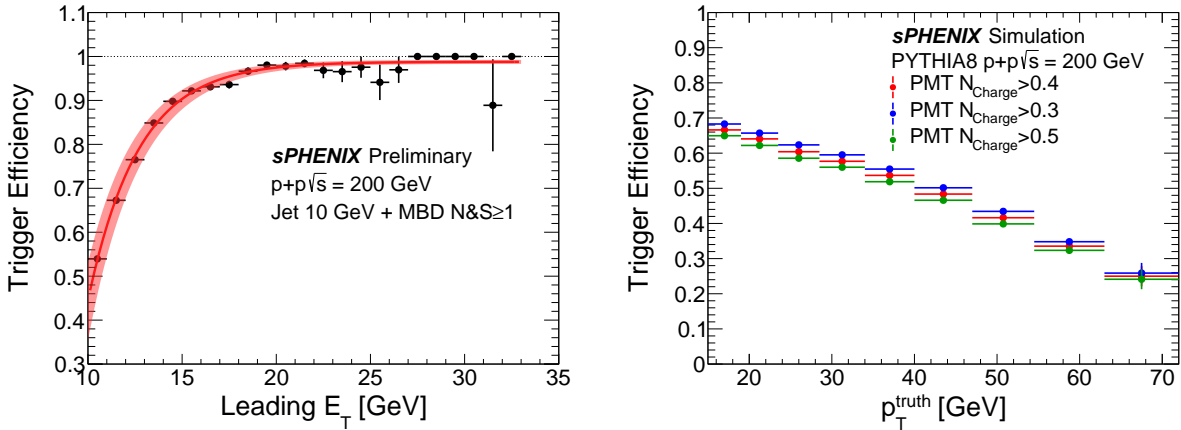


**Figure 1:** Left: Jet spectra from the 10 GeV trigger as a function of jet  $p_T$ . The red line is a fit to the data, and the shaded region around the fit are the upper and lower fit variations based on the fit uncertainties. Right: Minimum bias trigger efficiency measured in simulation. The different color markers on the right represent different MBD charge requirements of  $> 0.3$  (blue),  $> 0.4$  (red) and  $> 0.5$  (green).

The efficiency of the MB trigger requirement is evaluated in simulation, by analyzing PYTHIA-8 events in the MB, Jet 10 GeV, and Jet 30 GeV samples described above. The efficiency is determined by measuring the fraction of events that satisfy the event-level cuts in data (requiring a generator-level requirement of  $|z| < 30$  cm and at least one jet with  $|\eta^{\text{jet}}| < 0.7$ ) and also leave sufficient charge in the MBD to fire the minimum bias trigger. This efficiency correction also accounts for the disagreement between the minimum bias cross section produced by PYTHIA-8 and that measured via Vernier Scan [21] during the 2024 RHIC operational period, where it was measured to be 25.6 mb, approximately 61% of the total inelastic cross-section fo 42 mb.

The minimum bias trigger efficiency as measured in simulation can be seen in Figure 1 on the right. The MB trigger efficiency decreases with increasing jet  $p_T$ , and this occurs because as one approaches larger and larger values of momentum transfer  $Q^2$ , more of the longitudinal beam energy is converted to particle production at mid-rapidities, thus decreasing the amount of particle production at forward rapidities and the probability of firing the MBD trigger.

#### 4.4 Jet Energy Scale Calibration

To derive the jet energy scale calibration, particle-level truth jets are matched to reconstructed jets in simulation using the samples listed in Section 3. The matching between reconstructed and truth jets is performed using the criterion that the angular separation between the truth and reco jets has  $\Delta R = \sqrt{(\Delta\phi^2 + (\Delta\eta)^2)} < 0.3$ . For each matched truth-reco pair, the ratio  $p_T^{\text{reco}} / p_T^{\text{truth}}$  is calculated. The jet energy scale (JES),  $\langle p_T^{\text{reco}} / p_T^{\text{truth}} \rangle$ , as a function of  $p_T^{\text{truth}}$  is shown in Figure 2. As neither the EMCal nor HCal are fully calibrated the hadronic energy scale as mentioned earlier, the initial, non-unity of the JES is due to the non-compensating nature of the calorimeters.

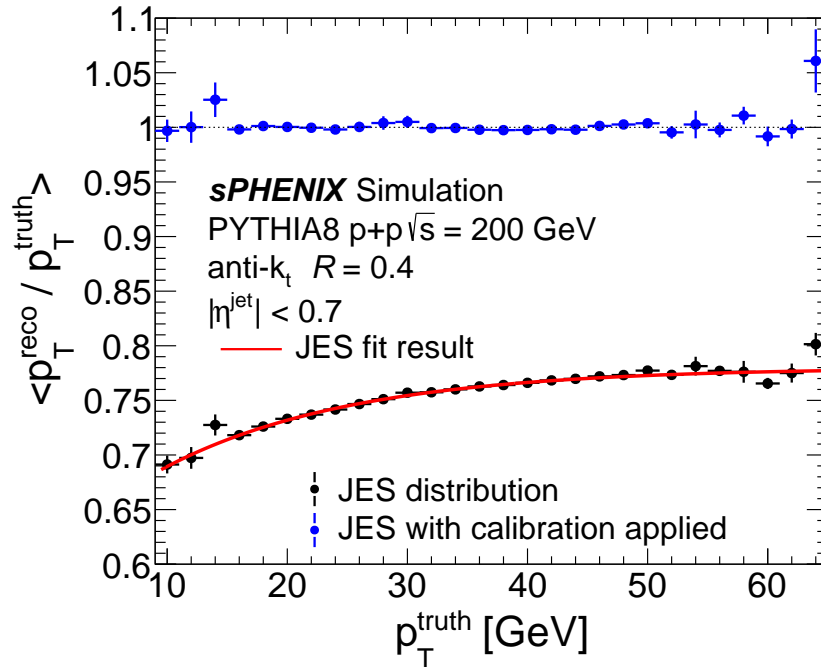


**Figure 2:** Black points: The uncalibrated JES as a function of  $p_T^{\text{truth}}$ . Blue points: The JES as a function of  $p_T^{\text{truth}}$  after the JES calibration has been applied.

The uncalibrated JES shown in Figure 2 in black is fit using a smooth, exponential function, and the jet energy scale is then calibrated by generating a mapping function from reconstructed jet  $p_T$  to truth jet  $p_T$  via numerical inversion [22] and applying the mapping to each reconstructed jet's  $p_T$ . A technical closure test of the JES calibration is shown in blue in Figure 2 and has an average non-closure of less than 1% independent of  $p_T^{\text{truth}}$

#### 4.5 Unfolding

In order to account for the impact of the finite JER and other detector effects on the measured yields, the JES-calibrated reconstructed jet spectrum is corrected using a Bayesian unfolding procedure [23] in the publicly available ROOUNFOLD package [20]. To build the response matrix, reconstructed jets must be matched to truth jets following the same selection criteria used for the JES calibration. The dijet bisector method [24] was used to quantify differences in the JER obtained in data and simulation. It was found that the simulation underestimated the jet resolution found in real data. Thus, before unfolding, all reconstructed jet  $p_T$  values in simulation received an additional, Gaussian smearing to match the JER estimated in data. The resulting response matrices, for each of the selections used to reject jet backgrounds, are shown in Figure 3.

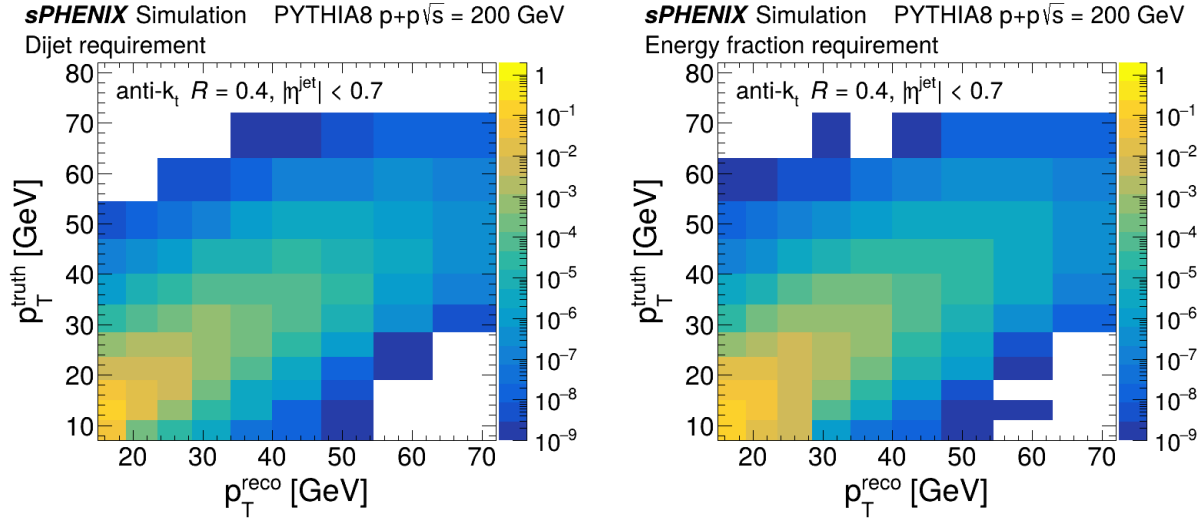


**Figure 3:** Response matrices used in the unfolding correction, with reconstructed jets after the JES calibration. The left and right plots are with the dijet method and with the energy fraction method, respectively, used to reject backgrounds as detailed in Section 4.2.

The unfolding procedure additionally corrects for both “fakes” (cases where the selected reconstructed jets have matching truth jets outside the fiducial acceptance) and “misses” (cases where the reconstructed jets are outside the kinematic selection, or are not selected due to jet- or event-level background rejection cuts). These corrections are typically 10% or smaller for the  $p_T$  range reported here. To unfold the data, the prior distribution and response matrix are reweighted so that the jet  $p_T$  distribution in simulation matches that in the data. The unfolded result is then corrected for the reconstruction and trigger efficiencies as described above.

## 5 Systematic Uncertainties

The main sources of systematic uncertainty considered in the measurement are the shape of the prior in the unfolding, the background rejection, the JES uncertainty, the JER uncertainty, the jet trigger efficiency, and the uncertainty on the MB trigger cross-section. These uncertainties are summarized below. The relative magnitude of all uncertainties relative to the nominal cross-section (evaluated as  $\frac{\mu - \sigma}{\mu}$ , where  $\mu$  is the nominal value and  $\sigma$  is the systematic uncertainty) are summarized in Figure 4. The systematic arising from the JES is the largest owing to a conservative estimation of the mismodeling of the hadronic response of the calorimeters in simulation and grows as a function of  $p_T$ . The systematics discussed here are taken as uncorrelated and summed in quadrature to attain the total systematic uncertainty.

The uncertainty on the shape of the prior is evaluated by repeating the unfolding procedure without reweighting the jet  $p_T$  spectrum in simulation to match that in data. The uncertainty in the background rejection is evaluated by considering the difference in the results produced with either of the two background rejection methods from the nominal (constructed by averaging the two results). The JES uncertainty is estimated to be approximately 6% for this preliminary analysis, and its impact is evaluated by shifting the reconstructed jet  $p_T$  up and down by this amount

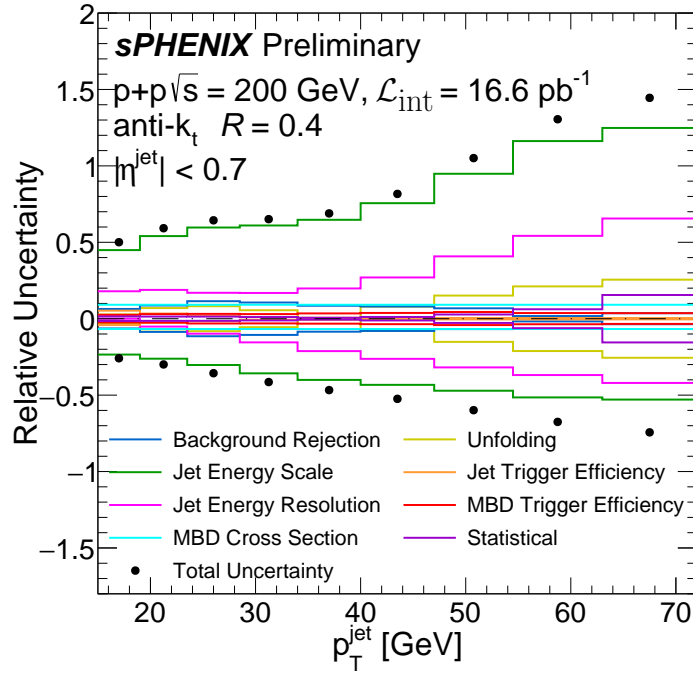


**Figure 4:** Summary of systematic uncertainties in the measurement, with each component shown as different color histograms and the total in black markers.

in simulation, generating new response matrices, and repeating the analysis. This uncertainty includes contributions from the absolute calibration of the EMCal via the  $\pi^0 \rightarrow \gamma\gamma$  peak in data and simulation, the relative calibration of the HCal via the minimum-ionizing particle distribution in cosmic data-taking and simulation, and in the absolute response of the calorimeter system to hadrons estimated in test beam [16].

The uncertainty in the JER is evaluated by considering larger or smaller degrees of smearing of the jet  $p_T$  in the simulation, compared to the nominal needed to match the resolution in data according to the bisector method. The uncertainty in the jet trigger efficiency is evaluated by varying the efficiency correction within the uncertainties in the fit in Figure 1. The uncertainties in the MBD cross-section for MB  $p+p$  events and its efficiency in jet events are evaluated as part of the Vernier scan analysis used to determine the central value and by varying the MBD thresholds in simulation as shown in the right side of Figure 1, respectively.

## 6 Results

The inclusive jet cross-section, measured with the combined sPHENIX electromagnetic and hadronic calorimeter system and fully corrected to particle level, is shown in Figure 5. For  $p_T > 50$  GeV, the relative statistical uncertainty point-to-point is approximately 20% or lower, demonstrating the statistical reach of the sPHENIX Run-24 dataset. The data are compared to a next-to-leading order (NLO) perturbative QCD (pQCD) calculation provided by Werner Vogelsang following the methodology used in Reference [25] (shown in red) as well as a PYTHIA-8 with

Detroit tune truth jet spectrum (shown in green). While it can be qualitatively assessed that the NLO calculation overestimates the cross-section, the calculation does not have a hadronization component. Ergo, an updated comparison with hadronization effects included will provide an apples-to-apples comparison. It should be noted however, that there is a  $p_T$  dependence to the agreement: the agreement is worse at low  $p_T$  and within systematic uncertainty at high  $p_T$ . For the pQCD calculation, the lower and upper bounds of the band represent renormalization scales of  $p_T/2$  and  $2p_T$ , respectively. The PYTHIA-8 truth jet spectrum agrees with the measured cross-section to within uncertainty until the two lowest  $p_T$  bins.

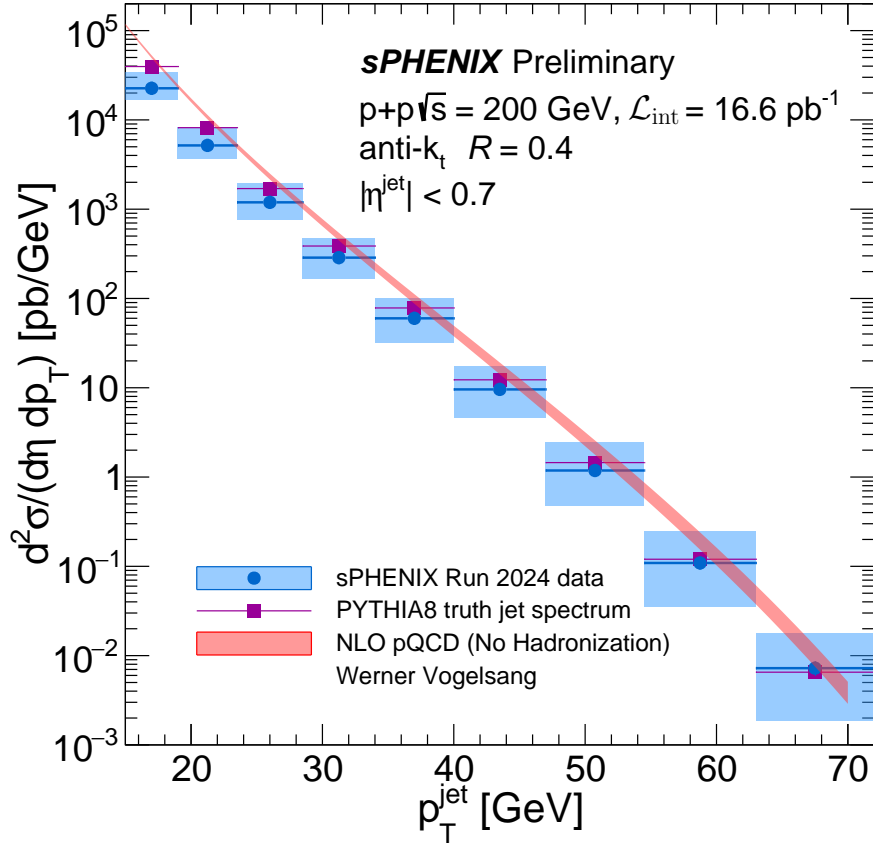


**Figure 5:** Unfolded jet cross-section for anti- $k_t$   $R=0.4$  jets measured by the sPHENIX full calorimeter system (blue circles), NLO pQCD calculation (red band), and a PYTHIA-8 Detroit-tune truth jet spectrum (purple squares). The blue, vertical bars and shaded boxes represent the statistical and systematic uncertainties, respectively, on the sPHENIX cross-section measurement. The statistical uncertainties are often smaller than the marker size. The NLO pQCD calculation does not include a hadronization step.

## 7 Summary

The fully unfolded, inclusive jet cross-section for anti- $k_t$   $R=0.4$  jets has been measured by the sPHENIX experiment at the Relativistic Heavy Ion Collider in  $p + p$  collisions at  $\sqrt{s} = 200 \text{ GeV}$ ,

using a combined electromagnetic and hadronic calorimeter system for the first time at RHIC at mid-rapidity. The measured cross-section is fully corrected for detector effects to the final-state particle level via unfolding, as well as for trigger and jet inefficiencies. This result will be improved upon by including the majority of the remaining luminosity collected during the 2024 operational period; though, it should be emphasized that this measurement offers better kinematic reach than any previous RHIC measurement, even with a portion of its statistics. Uncertainties related to the jet energy scale and jet energy resolution are expected to improve with better understanding of the calorimeter performance in Run 24 dataset.

## References

- [1] George Sterman and Steven Weinberg. Jets from quantum chromodynamics. *Phys. Rev. Lett.*, 39:1436–1439, Dec 1977. URL: <https://link.aps.org/doi/10.1103/PhysRevLett.39.1436>, doi:10.1103/PhysRevLett.39.1436. 1
- [2] B. I. Abelev *et al* (STAR Collaboration). Longitudinal double-spin asymmetry and cross section for inclusive jet production in polarized proton collisions at  $\sqrt{s} = 200$  GeV. *Phys. Rev. Lett.*, 97:252001, Dec 2006. URL: <https://link.aps.org/doi/10.1103/PhysRevLett.97.252001>, doi:10.1103/PhysRevLett.97.252001. 1
- [3] N. J. Abdulameer *et al* (PHENIX Collaboration). Measurement of inclusive jet cross section and substructure in  $p+p$  collisions at  $\sqrt{s_{NN}} = 200$  gev. 2024. URL: <https://arxiv.org/abs/2408.11144>, arXiv:2408.11144. 1
- [4] Gerald C. Blazey, Jay R. Dittmann, Stephen D. Ellis, V. Daniel Elvira, K. Frame, S. Grinstein, Robert Hiras, R. Piegai, H. Schellman, R. Snihur, V. Sorin, and Dieter Zeppenfeld. Run ii jet physics: Proceedings of the run ii qcd and weak boson physics workshop. 2000. URL: <https://arxiv.org/abs/hep-ex/0005012>, arXiv:hep-ex/0005012. 1
- [5] M. Cacciari, G. P. Salam, and G. Soyez. The anti-kt jet clustering algorithm. *Journal of High Energy Physics*, 2008(04):063–063, April 2008. URL: <http://dx.doi.org/10.1088/1126-6708/2008/04/063>, doi:10.1088/1126-6708/2008/04/063. 1
- [6] G. Aad *et al.* (ATLAS Collaboration). Measurements of jet cross-section ratios in 13 tev proton-proton collisions with ATLAS. *Physical Review D*, 110(7), October 2024. URL: <http://dx.doi.org/10.1103/PhysRevD.110.072019>, doi:10.1103/physrevd.110.072019. 1
- [7] A. Tumasyan *et al.* (CMS Collaboration). Measurement and QCD analysis of double-differential inclusive jet cross sections in proton-proton collisions at  $\sqrt{s} = 13$  TeV. *JHEP*, 02:142, 2022. [Addendum: *JHEP* 12, 035 (2022)]. arXiv:2111.10431, doi:10.1007/JHEP02(2022)142. 1
- [8] S. Acharya *et al* (ALICE Collaboration). Measurement of charged jet cross section in  $pp$  collisions at  $\sqrt{s} = 5.02$  TeV. *Phys. Rev. D*, 100:092004, Nov 2019. URL: <https://link.aps.org/doi/10.1103/PhysRevD.100.092004>, doi:10.1103/PhysRevD.100.092004. 1
- [9] A. Adare *et al* (PHENIX Collaboration). An Upgrade Proposal from the PHENIX Collaboration. 2015. arXiv:1501.06197. 2
- [10] R. Belmont *et al.* Predictions for the sPHENIX physics program. *Nucl. Phys. A*, 1043:122821, 2024. doi:10.1016/j.nuclphysa.2024.122821. 2

- [11] M. Harrison, T. Ludlam, and S. Ozaki. RHIC project overview. *Nucl. Instrum. Meth. A*, 499(2):235–244, 2003. doi:10.1016/S0168-9002(02)01937-X. 2
- [12] The sPHENIX Collaboration. sPHENIX Technical Design Report, PD-2/3 Release. 2019. URL: [https://indico.bnl.gov/event/7081/attachments/25527/38284/sphenix\\_tdr\\_20190513.pdf](https://indico.bnl.gov/event/7081/attachments/25527/38284/sphenix_tdr_20190513.pdf). 2
- [13] H. Klest. Overview and design of the sPHENIX TPC. *J. Phys. Conf. Ser.*, 1498:012025, 2020. arXiv:2110.02082, doi:10.1088/1742-6596/1498/1/012025. 2
- [14] S. Aune et al. The sPHENIX Micromegas Outer Tracker. *Nucl. Instrum. Meth. A*, 1066:169615, 2024. doi:10.1016/j.nima.2024.169615. 2
- [15] C. A. Aidala et al. Design and Beam Test Results for the 2-D Projective sPHENIX Electromagnetic Calorimeter Prototype. *IEEE Trans. Nucl. Sci.*, 68(2):173–181, 2021. doi:10.1109/TNS.2020.3034643. 2
- [16] C. A. Aidala et al. Design and Beam Test Results for the sPHENIX Electromagnetic and Hadronic Calorimeter Prototypes. *IEEE Trans. Nucl. Sci.*, 65(12):2901–2919, 2018. doi:10.1109/TNS.2018.2879047. 2, 5
- [17] T. G. O’Connor et al. Design and testing of the 1.5 T superconducting solenoid for the BaBar detector at PEP-II in SLAC. *IEEE Trans. Appl. Supercond.*, 9:847–851, 1999. doi:10.1109/77.783429. 2
- [18] Torbjörn Sjöstrand et al. An introduction to PYTHIA 8.2. *Comput. Phys. Commun.*, 191:159–177, 2015. arXiv:1410.3012, doi:10.1016/j.cpc.2015.01.024. 3
- [19] M. R. Aguilar, Z. Chang, R. K. Elayavalli, R. Fatemi, Y. He, Y. Ji, D. Kalinkin, M. Kelsey, I. Mooney, and V. Verkest. PYTHIA8 underlying event tune for RHIC energies. *Phys. Rev. D*, 105(1):016011, 2022. arXiv:2110.09447, doi:10.1103/PhysRevD.105.016011. 3
- [20] T. Adye. Unfolding algorithms and tests using RooUnfold. In *PHYSTAT 2011*, pages 313–318, Geneva, 2011. CERN. arXiv:1105.1160, doi:10.5170/CERN-2011-006.313. 3, 4, 5
- [21] S. van der Meer. Calibration of the effective beam height in the ISR. 1968. URL: <https://cds.cern.ch/record/296752>. 4, 3
- [22] A. Cukierman and B. Nachman. Mathematical Properties of Numerical Inversion for Jet Calibrations. *Nucl. Instrum. Meth. A*, 858:1–11, 2017. arXiv:1609.05195, doi:10.1016/j.nima.2017.03.038. 4, 4
- [23] G. D’Agostini. Improved iterative bayesian unfolding, 2010. URL: <https://arxiv.org/abs/1010.0632>, arXiv:1010.0632. 4, 5
- [24] G. Aad *et al* (ATLAS Collaboration). Jet energy resolution in proton-proton collisions at  $\sqrt{s} = 7$  TeV recorded in 2010 with the ATLAS detector. *Eur. Phys. J. C*, 73(3):2306, 2013. arXiv:1210.6210, doi:10.1140/epjc/s10052-013-2306-0. 4, 5
- [25] L. E. Gordon and W. Vogelsang. Polarized and unpolarized prompt photon production beyond the leading order. *Phys. Rev. D*, 48:3136–3159, Oct 1993. URL: <https://link.aps.org/doi/10.1103/PhysRevD.48.3136>, doi:10.1103/PhysRevD.48.3136. 6